Coordinated Volt-Var Control of Reconfigurable Microgrids with Power-to-Hydrogen Technologies

Khalil Gholami , Ali Azizivahed , Ali Arefi , Li Li , Mohammad Taufiqul Arif * , Md. Enamul Haque

Posted Date: 7 November 2024

doi: 10.20944/preprints202411.0460.v1

Keywords: Volt-VAr control; electric vehicles; network reconfiguration; power-to-hydrogen; hydrogen-to-power; electrolyzer; fuel cell

 doi:10.20944/preprints202411.0460.v1

Article

Coordinated Volt-Var Control of Reconfigurable Microgrids with Power-to-Hydrogen Technologies

Khalil Gholami [1], Ali Azizivahed [2], Ali Arefi [3], Li Li [2], Mohammad Taufiqul Arif [1,*] and Md Enamul Haque [1]

[1] Renewable Energy and Electric Vehicle (REEV) Lab, School of Engineering, Deakin University, Geelong, VIC 3216, Australia
[2] School of Electrical and Data Engineering, University of Technology Sydney, Sydney, Australia
[3] School of Engineering and Energy, Murdoch University, Perth, Australia
* Correspondence: m.arif@deakin.edu.au

Abstract: This paper seeks to enhance volt-var control strategies within reconfigurable microgrids by integrating innovative technologies of power-to-hydrogen (P2H) via electrolyzers and hydrogen-to-power (H2P) through fuel cells. Specifically, it focuses on the simultaneous coordination of electrolyzer, hydrogen storage, and fuel cell alongside on-load tap changers, smart PV inverters, renewable energy sources, diesel generators, and electric vehicle aggregation (EVA) within the microgrid system. Additionally, dynamic network reconfiguration is employed to enhance microgrid flexibility, facilitate power sharing, and improve the overall system adaptability. Given the inherent unpredictability linked to resources, the unscented transformation method is employed to account for these uncertainties in the proposed volt-var control strategy. Finally, the model is formulated as a convex optimization problem and is solved by GUROBI, which leads to having a time-efficient volt-var model with high accuracy. To assess the effectiveness of the model, it is eventually examined on a modified 33-bus microgrid in several cases. Through the results of the under-study microgrid, the developed volt-var control is a great remedy to the simultaneous operation of EVA, P2H and H2P in reconfigurable microgrids with flatter voltage profile across the microgrid.

Keywords: Volt-VAr control; electric vehicles; network reconfiguration; power-to-hydrogen; hydrogen-to-power; electrolyzer; fuel cell

1. Introduction

Microgrids, primarily powered by abundant renewable energy sources (RESs), can serve as smart grid components to enhance the reliability of the overall network [1] as well as effecting the market price fluctuations [2]. Additionally, the adoption of diverse technologies, such as electric vehicle aggregators (EVAs) and hydrogen generation through electrolyzers, followed by conversion back to electricity via fuel cells, has significantly increased due to their eco-friendly nature. However, as the number of RESs, EVAs, and conversions between hydrogen and power grows, microgrids may experience voltage fluctuations, leading to technical and economic challenges for microgrid operators and customers alike. To overcome the disturbances related to voltages, the concept of volt-var control is appealed. Volt-var means developing a strategy to simultaneously manage different equipment, including on-load tap changer (OLTC), switchable capacitor banks (SCBs), diesel generators (DGs), smart inverters and so on to maintain the voltage of network within acceptable ranges.

There are various volt-var control techniques in the literature which are discussed as follows. One of the most well-known devices which has always been used in controlling voltage in power grids is SCB [3] because of its affordable cost in the market. OLTC [4] is another conventional device frequently used to control the voltage of the network due to its reasonable cost and effective applicability. Smart PV inverters (SPIs) are novel technology which can be a great remedy to be used in volt-var control strategies, because they have a fast response under different conditions and do not

 doi:10.20944/preprints202411.0460.v1

inject any harmonics into the grid [5]. Authors in [6,7] got energy storage systems (ESSs) managed to mitigate over-/under-voltage issues in distribution grids by developing a coordinated charging/discharging scheme. Soft open point is another electronic-based technique used in voltage management in distribution grids [8]. Coordinating volt-var with demand response programs was investigated in [9]. It is clear that current distribution grids have been equipped with various technologies to control voltage and reactive power. Although this enhances the flexibility to have a secure system, coordination among them entails up-to-date tools.

Electric vehicles are cutting-edge technologies which are penetrated in power system operational and planning schemes. In terms of EVAs in volt-var control, some investigations have been conducted so far. To illustrate this, Ref. [10] developed a coordination approach for electric vehicle charging stations, dispatchable generation sources, and energy storage units in distribution grids. Similarly, in [11], the volt-var control was developed in distribution grids in the presence of electric vehicles, renewable resources, capacitors and OLTC. Besides, the reactive power provision by electric vehicle charging stations was deployed to manage the voltage stability index in distribution networks [12]. Through the mentioned papers, electric vehicles have been investigated in volt-var schemes, but there are some gaps which need to be tackled. To begin with, extensive volt-var devices were not considered. Secondly, the technology of vehicle-to-grid and grid-to-vehicle EVAs has not been studied adequately. Thirdly, network reconfiguration has not been involved. Fourthly, uncertainties have not been studied thoroughly.

Feeder reconfiguration is a cutting-edge capability of smart grids which can be used at distribution level for different purposes. For example, authors of [13] implemented the network reconfiguration and capacitor allocation for volt-var control of distribution grids by using a population-based algorithm. On the same track, modified gray wolf optimization was used to assess the impact of feeder reconfiguration on volt-var control of distribution grids in [14]. From this research, it can be seen that simultaneous feeder reconfiguration and PV inverter management result in higher energy savings. Ref. [15] concentrated on volt-var control in reconfigurable droop-based islanded microgrids with the aim of power loss minimization. Compared to the references mentioned, this paper uses convex-formulation which enables operators to reach the possible global solution, but it did not consider different volt-var control equipment such as smart PV inverters, EVAs, and so on. Although there are a few feeder reconfigurations in volt-var control schemes, some factors have not been sufficiently addressed, such as coordination of EVAs aggregations, suitable uncertainty modeling, and so on. Accordingly, developing a mathematical framework for reaching an extensive volt-var control in reconfigurable microgrids with considering the coordination of EVAs entails further assessments.

Power-to-hydrogen (P2H) and hydrogen-to-power (H2P) technologies are typically implemented using electrolyzers and fuel cells [16,17]. Consequently, some researchers have focused on energy management within microgrids that incorporate these technologies to reach the net-zero target soon. For example, researchers in [18] proposed a method for determining the optimal size of concentrated solar power systems intended for hydrogen refueling stations. The resilience of microgrids utilizing the P2H concept was examined in [19] for their operation in islanded mode. A stochastic energy management strategy, utilizing the particle swarm optimization algorithm, was also explored for operating hydrogen-based microgrids in both islanded and grid-connected modes in [20]. It is shown that H2P and P2H will play a main role in future power systems. However, their effects on the volt-var management have not been investigated adequately.

Considering the fact that volt-var control includes some uncertain parameters such as load, renewable resources and so on, assessing the impact of such uncertain parameters on the model output should be investigated. So far, several investigations have been conducted in literature. To begin with, authors of [21] used a stochastic framework, namely Monte Carlo Simulation, to capture the uncertainties related to the arrival and departure times and charging demand of EVAs. Even though Monte Carlo Simulation provides highly accurate results, it is assigned to the time-consuming techniques because of taking extensive scenarios into account. Volt-var control operates in real-time, which significantly limits the feasibility of using Monte Carlo Simulation. To overcome this issue, in

 doi:10.20944/preprints202411.0460.v1

[22], authors modeled the influence of uncertainties on the volt-var control by point estimation technique which is not computationally expensive. It is worthwhile that point estimation method is computationally friendly, but it assumes the input uncertain parameters are independent to each other and there is not any correlation among them [23]. In order to tackle this drawback, unscented transformation (UT) method [24], which can model the correlation among input uncertain parameters, has been introduced. Considering uncertainties plays a key role in volt-var control approaches. Toward this end, in this research, UT method is utilized to model the uncertainties related to the loads, RESs, and EVAs.

To the best of the knowledge of the authors, developing a volt-var control which simultaneously addresses the following aspects is still necessary in the literature.

- Developing a comprehensive volt-var control by effectively managing various equipment such as OLTC, SCBs, RESs, smart PV inverters (SPVIs), etc.;
- Incorporating the concepts of P2H and H2P into the volt-var control by electrolyzer, hydrogen storage and fuel cell;
- Incorporating the concept of grid-to-vehicle and vehicle-to-grid of EVA in the volt-var control of reconfigurable microgrids;
- Implementing the dynamic feeder reconfiguration in the presence of coordinating other equipment to increase the flexibility of the microgrids;
- Thoroughly considering the unpredictability and intermittency regarding loads, RESs, and EVAs by the UT method in order to evaluate the suggested volt-var control in a realistic manner;
- Developing the volt-var control possesses convex formulation which results in finding the possible global solution in a finite time.

The rest of the paper is organized as follows. Section 2 discusses the problem formulation. The UT method is described in Section 3 to model the uncertainties. The results are provided in Section 4, followed by a conclusion in Section 5.

2. Problem Formulation

A microgrid (MG) is a localized energy system that integrates various renewable energy sources, energy storage units, and conventional generators. It can be configured to adapt to changing conditions through the incorporation of remote switches. Key components of the considered microgrid include the following cutting-edge technologies:

- **SPVIs**: Convert the direct current output from solar panels into alternating current and provide or absorb reactive power.
- **OLTCs**: Regulate voltage levels by adjusting the tap positions on transformers, which are generally installed after the slack bus.
- **Electrolyzers**: Generate hydrogen by converting electrical power into hydrogen through water electrolysis.
- **Fuel cells:** Convert stored hydrogen back into electricity.
- **Hydrogen Storage:** A tank located between the electrolyzer and fuel cell that enhances flexibility by storing hydrogen generated from surplus renewable energy for use by the fuel cell.
- **EVAs**: Aggregations of EVs that are used as mobile energy storage systems.
- **DGs**: Diesel generators that are typically deployed to meet loads when renewable energy sources do not provide sufficient generation.
- **Remote Switches**: These switches enable microgrid operators to change the configuration of the microgrid to enhance its techno-economic efficiency.

This investigation aims for the cost-efficient operation of grid-connected microgrids by minimizing expenses related to power trading in energy markets, energy production, and equipment operations. Furthermore, electrolyzers and fuel cells are effectively integrated into the volt-var control model, allowing for an assessment of their impact on the microgrid's voltage stability. It also applies network reconfiguration to optimize power flow and enhance overall efficiency.

The following subsections define the proposed objective function which is followed by various constraints related to the microgrids' equipment, such as SPVIs, OLTC, electrolyzer, fuel cell, etc.

 doi:10.20944/preprints202411.0460.v1

2.1. Objective Function

The objective function (OF) of the suggested volt-var control is mathematically defined as follows. In this OF, there are 6 terms [9]. The first one is related to the cost of purchasing energy from the wholesale market. The cost of power generation by DGs is shown in the second term. The cost of switching OLTC and SCB are referred to in terms three and four, respectively. The costs of charging and discharging of EVA and hydrogen system are presented in the fifth and sixth terms, respectively.

$$\begin{aligned} OF = & \overbrace{\sum_{t\in\Omega_{time}} \lambda_{SS}^{t} P_{SS}^{t} \Delta t}^{1} + \overbrace{\sum_{d\in\Omega_{dg}} \sum_{t\in\Omega_{time}} \lambda_{DG}^{d,t} P_{DG}^{d,t} \Delta t}^{2} \\ & + \overbrace{\sum_{o\in\Omega_{oltc}} \sum_{t\in\Omega_{time}} \lambda_{oltc}^{o} \left| Tap_{oltc}^{o,t} - Tap_{oltc}^{o,t-1} \right|}^{3} \\ & + \overbrace{\sum_{c\in\Omega_{cb}} \sum_{t\in\Omega_{time}} \lambda_{CB}^{c} \left| \psi_{CB}^{c,t} - \psi_{CB}^{c,t-1} \right|}^{4} \\ & + \overbrace{\sum_{e\in\Omega_{eva}} \sum_{t\in\Omega_{time}} \lambda_{SS}^{t} \left(P_{ch,eva}^{e,t} - P_{dis,eva}^{e,t} \right) \Delta t}^{5} \\ & + \overbrace{\sum_{h\in\Omega_{hgn}} \sum_{t\in\Omega_{time}} \lambda_{SS}^{t} \left(P_{elsr}^{h,t} - P_{FC}^{h,t} \right) \Delta t}^{6} \end{aligned} \quad (01)$$

2.2. List of Constraints

Constraints are a mandatory part of optimization problems for establishing reliable models. With regard to the volt-var control, predominant constraints, including SPVIs, SCBs, OLTCs, EVAs, and H2P/P2H conversions, are elaborated in the following subsections.

2.2.1. Smart PV Inverters

SPVI is an emerging technology that has gained attention from researchers due to its ability to mitigate voltage fluctuations by injecting or absorbing reactive power into the grid [25]. This concept of the smart inverter can be modeled into the volt-var control by the following constraints.

$$Q_{PV}^{p,t} \le \sqrt{\left(S_{PV}^{p}\right)^2 - \left(P_{PV}^{p,t}\right)^2}, \forall t \in \Omega_{time}, \forall p \in \Omega_{PV} \quad (02)$$

$$Q_{PV}^{p,t} \ge -\sqrt{\left(S_{PV}^{p}\right)^2 - \left(P_{PV}^{p,t}\right)^2}, \forall t \in \Omega_{time}, \forall p \in \Omega_{PV} \quad (03)$$

2.2.2. Electric Vehicles

To achieve the net-zero target in the near future, EVAs have been implemented. These environmentally friendly solutions can undoubtedly replace fuel-based transportation systems. Consequently, there will be extensive integration of EVs in power grids. However, if operated in an uncoordinated manner, the network is likely to experience voltage disturbances. Therefore, a set of constraints must be satisfied in the vol-var control problem. Constraint (04) is related to the energy of EVA. The energy of EVA must remain within its maximum and minimum capacities as guaranteed by (05). The charging and discharging of EVA are regulated by constraints (06) and (07), respectively. Additionally, constraint (08) ensures that the energy at the start and end of a 24-hour period remains equal.

$$E_{eva}^{e,t} = E_{eva}^{e,t-1} + \eta_{ch} P_{ch,eva}^{e,t} \Delta t - \left(\frac{1}{\eta_{dis}}\right) P_{dis,eva}^{e,t} \Delta t \ , \forall t \in \Omega_{time} \text{ and } t > 1, \forall e \in \Omega_{eva} \quad (04)$$

$$E_{eva}^{e,min} \le E_{eva}^{e,t} \le E_{eva}^{e,max}, \forall t \in \Omega_{time}, \forall e \in \Omega_{eva} \quad (05)$$

 doi:10.20944/preprints202411.0460.v1

$$P_{ch,eva}^{e,min} \le P_{ch,eva}^{e,t} \le P_{ch,eva}^{e,max}, \forall t \in \Omega_{time}, \forall \mathrm{e} \in \Omega_{eva} \quad (06)$$

$$P_{dis,eva}^{e,min} \le P_{dis,eva}^{e,t} \le P_{dis,eva}^{e,max}, \forall t \in \Omega_{time}, \forall \mathrm{e} \in \Omega_{eva} \quad (07)$$

$$E_{eva}^{e,initial} = E_{eva}^{e,final}, \text{e. g. }, initial = 0, final = 24, \forall \mathrm{e} \in \Omega_{eva} \quad (08)$$

2.2.3. Switchable Capacitor Banks

SCBs are an essential component of volt-var control schemes due to their cost efficiency and ability to effectively compensate for the reactive power in the network [26]. To schedule the on/off status of SCBs, the following constraints are considered.

$$Q_{CB}^{c,t} = \psi_{CB}^{c,t} Q_{rate}^{c}, \forall t \in \Omega_{time}, \forall c \in \Omega_{cb} \quad (09)$$

$$0 \le \psi_{CB}^{c,t} \le \psi_{CB}^{c,Max}, \forall t \in \Omega_{time}, \forall c \in \Omega_{cb} \quad (10)$$

2.2.4. On-Load Tap Changer

OLTC is typically installed in the upstream network, and its main function is to regulate the network's voltage level from the slack bus perspective [27]. Consequently, the OLTC tap position must be constrained within allowable limits, as defined by the following constraint.

$$T_{oltc}^{o,min} \le T_{oltc}^{o,t} \le T_{oltc}^{o,max}, \forall t \in \Omega_{time}, \forall o \in \Omega_{oltc} \quad (11)$$

2.2.5. Diesel Generator

DGs typically consume fuel to generate power. These dispatchable units can be employed for various purposes, such as supporting specific loads, reducing operational costs and so on. Given that DGs have limited generation capacity, their output is constrained between maximum and minimum values, as specified by constraint (12). Additionally, the output of DGs cannot fluctuate rapidly over different intervals; therefore, their ramp-rate limitation is enforced through constraint (13).

$$P_{DG}^{d,min} \le P_{DG}^{d,t} \le P_{DG}^{d,max}, \forall t \in \Omega_{time}, \forall d \in \Omega_{dg} \quad (12)$$

$$R_{DG}^{d,Down} \le P_{DG}^{d,t} - P_{DG}^{d,t-1} \le R_{DG}^{d,Upper}, \forall t \in \Omega_{time}, \forall d \in \Omega_{dg} \quad (13)$$

2.2.6. Hydrogen-to-Power Conversion Technology

The generation of green hydrogen depends on electrolyzers that convert electricity into hydrogen, a process commonly referred to as P2H. This hydrogen can subsequently be converted back into electricity through fuel cells, a process known as H2P. It is notable that hydrogen storage plays a crucial role in this cycle, enabling surplus energy generated from renewable sources to be stored as hydrogen and later utilized during periods of higher load demand, elevated market prices, or other needs [28–30]. The mathematical formulation of the P2H and H2P concepts is described as follows. Initially, the state of hydrogen in the h^{th} hydrogen storage unit for $t = 1$ and $t > 1$ is represented by constraints (14) and (15), respectively. The electricity consumed by the electrolyzer to produce hydrogen is determined by constraint (16). Similarly, the power generated by the fuel cell is calculated using constraint (17). Eqs. (18) and (19) define the operational limits for the fuel cell and electrolyzer, respectively. Constraint (20) guarantees that the hydrogen state remains within its allowable range. Lastly, Eq. (21) ensures that the amount of stored hydrogen at the end of the cycle (e.g., the 24th hour) is equal to the amount stored at the beginning of the cycle.

$$S_{hgn}^{h,1} = S_{hgn}^{h,t^{initial}} + H_{elsr}^{h,1} \Delta t - H_{FC}^{h,1} \Delta t, \quad \forall h \in \Omega_{hgn} \quad (14)$$

$$S_{hgn}^{h,t} = S_{hgn}^{h,t-1} + H_{elsr}^{h,t} \Delta t - H_{FC}^{h,t} H_{FC}^{h,t} \Delta t, \quad \forall t > 1, \quad t \in \Omega_{time}, \quad \forall h \in \Omega_{hgn} \quad (15)$$

$$P_{elsr}^{h,t} = \frac{\Psi_{eih} \times H_{elsr}^{h,t}}{\eta_{elsr}}, \quad \forall t \in \Omega_{time}, \forall h \in \Omega_{hgn} \quad (16)$$

 doi:10.20944/preprints202411.0460.v1

$$H_{FC}^{h,t} = \frac{P_{FC}^{h,t}}{\eta_{FC} \times \Psi_{eih}}, \qquad \forall t \in \Omega_{time}, \forall h \in \Omega_{hgn} \tag{17}$$

$$P_{FC}^{h,min} \le P_{FC}^{h,t} \le P_{FC}^{h,max}, \qquad \forall t \in \Omega_{time}, \forall h \in \Omega_{hgn} \tag{18}$$

$$P_{elsr}^{h,min} \le P_{elsr}^{h,t} \le P_{elsr}^{h,max}, \qquad \forall t \in \Omega_{time}, \forall h \in \Omega_{hgn} \tag{19}$$

$$S_{hgn}^{h,\min} \le S_{hgn}^{h,t} \le S_{hgn}^{h,\max}, \qquad \forall t \in \Omega_{time}, \forall h \in \Omega_{hgn} \tag{20}$$

$$S_{hgn}^{h,t^{initial}} = S_{hgn}^{h,t^{final}}, \qquad \text{e.g.}, t^{initial} = 0, t^{final} = 24, \forall h \in \Omega_{hgn} \tag{21}$$

2.2.7. Power Flow

Network-constrained volt-var control is central to volt-var optimization, and it is modeled through the following constraints [31–33], with reconfiguration discussed in [34,35]. Constraints (22) and (23) balance the real and reactive power in the network. To calculate the voltage of each bus, constraints (24) and (25) are utilized [32,35,36]. The power flow of the opened switches must be zero, as modeled in Eqs. (26) and (27). The active and reactive power demands and generation at each bus are modeled by constraints (28) and (29), respectively. Maintaining network voltage within acceptable ranges is enforced by (30). Constraint (31) ensures that branch capacities do not exceed their allowable limits.

$$P_{net}^{n,t} = \sum_{m \in \Omega_{par_n}} P_{flow}^{mn,t} - \sum_{k \in \Omega_{chil_n}} P_{flow}^{nk,t}, \forall t \in \Omega_{time}, \forall n \in \Omega_{bus} \tag{22}$$

$$Q_{net}^{n,t} = \sum_{m \in \Omega_{par_n}} Q_{flow}^{mn,t} - \sum_{k \in \Omega_{chil_n}} Q_{flow}^{nk,t}, \forall t \in \Omega_{time}, \forall n \in \Omega_{bus} \tag{23}$$

$$V_b^{m,t} - V_b^{n,t} \le (1 - \alpha^{mn,t})\mathrm{M}_{big} + \left(R_L^{mn,t} P_{flow}^{mn,t} + X_L^{mn,t} Q_{flow}^{mn,t}\right)/V_{s_0}, \forall t \in \Omega_{time}, \forall n, m \in \Omega_{bus} \tag{24}$$

$$V_b^{m,t} - V_b^{n,t} \ge (\alpha^{mn,t} - 1)\mathrm{M}_{big} + \left(R_L^{mn,t} P_{flow}^{mn,t} + X_L^{mn,t} Q_{flow}^{mn,t}\right)/V_{s_0}, \forall t \in \Omega_{time}, \forall n, m \in \Omega_{bus} \tag{25}$$

$$-\mathrm{M}_{big}\alpha^{mn,t} \le P_{flow}^{mn,t} \le \mathrm{M}_{big}\alpha^{mn,t}, \qquad \forall t \in \Omega_{time}, \forall n, m \in \Omega_{bus} \tag{26}$$

$$-\mathrm{M}_{big}\alpha^{mn,t} \le Q_{flow}^{mn,t} \le \mathrm{M}_{big}\alpha^{mn,t}, \qquad \forall t \in \Omega_{time}, \forall n, m \in \Omega_{bus} \tag{27}$$

$$P_{net}^{n,t} = P_L^{n,t} - P_{DG}^{d,t} - P_{PV}^{p,t} + P_{ch,eva}^{e,t} - P_{dis,eva}^{e,t} + P_{elsr}^{h,t} - P_{FC}^{h,t}, \forall t \in \Omega_{time}, \forall n \in \Omega_{bus}, \forall d \in \Omega_{dg}, \forall p \in \Omega_{PV}, \forall e \in \Omega_{eva}, \forall h \in \Omega_{hgn} \tag{28}$$

$$Q_{net}^{n,t} = Q_L^{n,t} - Q_{DG}^{d,t} - Q_{PV}^{p,t} - Q_{CB}^{c,t}, \forall t \in \Omega_{time}, \forall n \in \Omega_{bus}, \forall d \in \Omega_{dg}, \forall p \in \Omega_{PV}, \forall c \in \Omega_{cb} \tag{29}$$

$$\left(V_b^{n,min}\right) \le V_b^{n,t} \le (V_b^{n,max}), \forall t \in \Omega_{time}, \forall n \in \Omega_{bus} \tag{30}$$

$$\left(P_{flow}^{mn,t}\right)^2 + \left(Q_{flow}^{mn,t}\right)^2 \le \left(S_{flow}^{mn,Max}\right)^2, \forall t \in \Omega_{time}, \forall n, m \in \Omega_{bus} \tag{31}$$

 doi:10.20944/preprints202411.0460.v1

2.2.8. Radiality of Network

The network must maintain a radial configuration during optimization, which means the network does not have any loops. This can be achieved by spanning tree conditions [37,38]. Eq. (32) ensures that the number of closed switches equals the number of buses minus one. Eq. (33) specifies that a line is included in the spanning tree if bus m serves as the parent of bus n, or if bus n serves as the parent of bus m. Eq (34) ensures that each bus, apart from the slack bus, is assigned exactly one parent. Eq. (35) signifies that the slack bus does not have any parents.

$$\sum_{mn\in\Omega_{branch}} \alpha^{mn} = |\Omega_{bus}| - 1\,, \qquad \alpha^{mn} \in \{0,1\} \tag{32}$$

$$\varphi^{m,n} + \varphi^{n,m} = \alpha^{mn}, \qquad \forall n,m \in \Omega_{bus}, \forall mn \in \Omega_{branch} \tag{33}$$

$$\sum_{m\in N(n)} \varphi^{m,n} = 1, \qquad \forall n,m \in \Omega_{bus} \tag{34}$$

$$\varphi^{1,n} = 0, \qquad \forall n \in \Omega_{bus} \tag{35}$$

3. Unscented Transformation

Generally, three main measures are used to evaluate the impact of uncertainties on the models: 1) Monte Carlo simulation [12], 2) analytic approaches and 3) approximation methods [39,40]. The primary drawback of the first method is the substantial number of trials required for convergence. The second approach, while fast and accurate, depends on precise mathematical assumptions to simplify problems. To address the limitations of both, the third approach that is more advantageous has been therefore introduced. The most well-known approximation approach is the UT method, which has proven to be an effective tool for estimating uncertainties in nonlinear correlated transformations [39,40]. The UT method offers several benefits, including ease of programming, simplicity, strong capacity for capturing uncertainties, low computational demands, and effective simulation of uncertainties in correlated scenarios [39,40]. To illustrate this approach, consider a general probabilistic problem expressed as $Y = fit(X)$, where Y denotes the output, fit provides the value of the objective function, and X represents the uncertain input parameters. Let Ω_{up} be the set of these uncertain parameters, X be a vector of length $|\Omega_{up}|$, characterized by a mean value (μ_x) and a covariance matrix C_{xx}. In this matrix, the diagonal components represent the variance of the uncertain parameters, while the off-diagonal components indicate the covariances between them. The UT method simulates uncertainties for $|\Omega_{up}|$ parameters with only $2|\Omega_{up}|+1$ evaluations, significantly reducing computational complexity. This method consists of the following steps:

1) Based on the input uncertain parameters, $2|\Omega_{up}|+1$ sample points are generated using the following expression:

$$S_p^l = \mu_x + \left(\sqrt{\frac{|\Omega_{up}|}{1-W_0}C_{xx}}\right)_l, \qquad l = 1,2,\dots,|\Omega_{up}| \tag{36}$$

$$S_p^{l+|\Omega_{up}|} = \mu_x - \left(\sqrt{\frac{|\Omega_{up}|}{1-W_0}C_{xx}}\right)_l, \quad l = 1,2,\dots,|\Omega_{up}| \tag{37}$$

$$S_p^{2|\Omega_{up}|+1} = \mu_x \tag{38}$$

In the preceding expressions, the term $(B)_l$ represents the l-th row or column of matrix B.

 doi:10.20944/preprints202411.0460.v1

2) For every generated sample point, the corresponding weighting factor is determined using the following equations:

$$W^l = \frac{1 - W_0}{2|\Omega_{up}|}, \qquad l = 1,2, \dots, |\Omega_{up}| \tag{39}$$

$$W^{l+|\Omega_{up}|} = \frac{1 - W_0}{2|\Omega_{up}|}, \qquad l = 1,2, \dots, |\Omega_{up}| \tag{40}$$

$$W^{2|\Omega_{up}|+1} = W_0 \tag{41}$$

3) Solve the proposed problem for the $2|\Omega_{up}| + 1$ samples generated above to compute the fitness function for each sample point, as follows.

$$Y^l = fit(S_p^l) \ , \qquad l = 1,2, \dots, 2|\Omega_{up}| + 1 \tag{42}$$

4) Determine the mean μ_y and the covariance C_{yy} of the output variable Y using the following formulas:

$$\mu_y = \sum_{l=1}^{2|\Omega_{up}|+1} W^l Y^l \tag{43}$$

$$C_{yy} = \sum_{l=1}^{2|\Omega_{up}|+1} W^l (Y^l - \mu_y)(Y^l - \mu_y)^T \tag{44}$$

4. Simulation Results

4.1. System Description

The performance of the suggested volt-var control is analyzed on a reconfigurable 33-bus microgrid [41], as illustrated in **Error! Reference source not found.**. This microgrid has been equipped with various devices as follows. To begin with, an OLTC is immediately installed after the upstream network with ten tap positions, e.g., five step-up and five step-down bands. Four PV resources are allocated at buses 15, 22, 24 and 33 by 500kVA inverters, respectively; their forecasted active powers are shown in **Error! Reference source not found.**. Three switchable capacitor banks, which possess 3 steps of 500kVAr, are dedicated at buses 5, 10 and 30, respectively. Diesel generators, another generation source, are placed at buses 7 and 13 with a capacity of 200kW, respectively. There are also two EVAs with their specifications in Table 1 and trip paths in **Error! Reference source not found.** and Table 2. The forecasted values of active and reactive demands are demonstrated in **Error! Reference source not found.** and **Error! Reference source not found.**, respectively. Two hydrogen systems, each equipped with an electrolyzer, hydrogen storage, and fuel cell, are located at buses 21 and 32. The electrolyzers and fuel cells both have a capacity of 200 kW. Additionally, each hydrogen storage unit has a maximum capacity of holding 200 kg of hydrogen. The forecasted market price is illustrated in **Error! Reference source not found.**.

The framework is evaluated under the following cases:

- Case 1: RESs (yes), DGs (yes), SCBs (yes), OLTC (yes), EVA (no), reconfiguration (no), electrolyzer (no), hydrogen storage (no), fuel cell (no).
- Case 2: RESs (yes), DGs (yes), SCBs (yes), OLTC (yes), EVA (yes), reconfiguration (no), electrolyzer (no), hydrogen storage (no), fuel cell (no).
- Case 3: RESs (yes), DGs (yes), SCBs (yes), OLTC (yes), EVA (yes), reconfiguration (yes), electrolyzer (no), hydrogen storage (no), fuel cell (no).
- Case 4: RESs (yes), DGs (yes), SCBs (yes), OLTC (yes), EVA (yes), reconfiguration (yes), electrolyzer (yes), hydrogen storage (yes), fuel cell (yes).

Preprints.org (www.preprints.org) | NOT PEER-REVIEWED | Posted: 7 November 2024 doi:10.20944/preprints202411.0460.v1

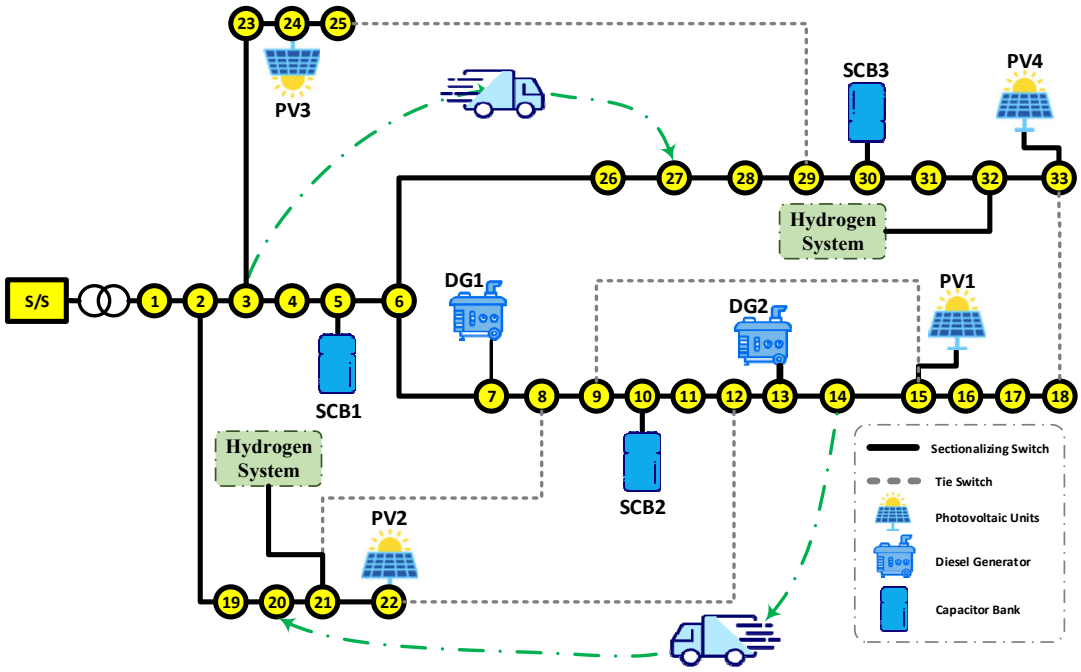

Figure 1. Schematic of 33-bus microgrid.

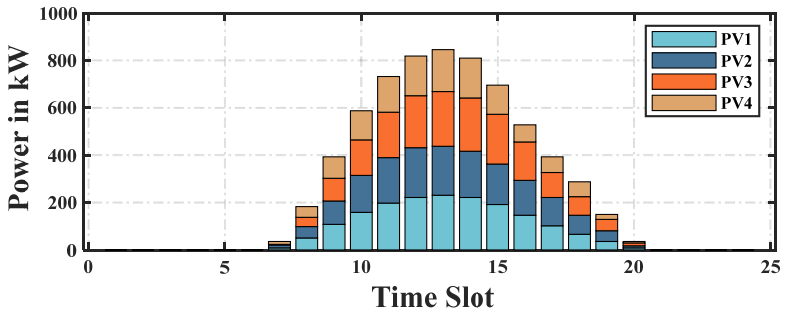

Figure 2. Forecasted values of PV resources.

Table 1. EVAs' specification.

EVA	Capacity (kWh)		Charge/Discharge(kW)	
	min	max	min	max
1	50	2000	200	200
2	50	2000	200	200

Table 2. EVAs' trip specification.

EVA	Trip 1				Trip 2			
	Departure		Arrival		Departure		Arrival	
	Time	bus	Time	bus	Time	bus	Time	bus
1	8	14	9	24	18	24	19	14
2	8	3	9	27	18	27	19	3

 doi:10.20944/preprints202411.0460.v1

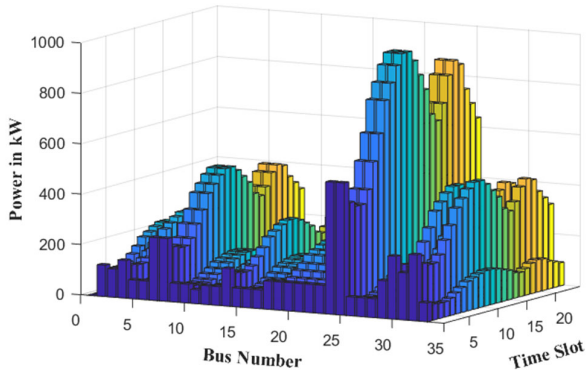

Figure 3. Forecasted active power of microgrid.

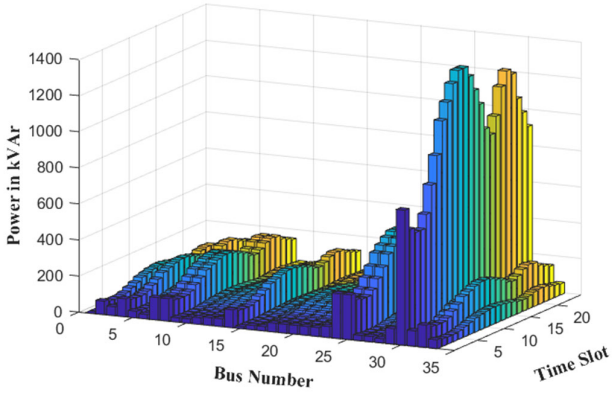

Figure 4. Forecasted reactive power of microgrid.

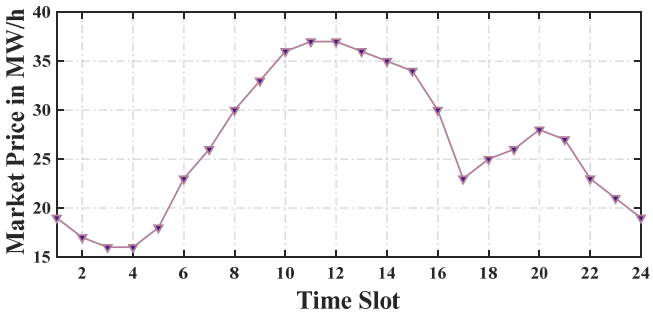

Figure 5. Forecasted electricity market price.

4.2. Numerical Results and Discussion

In this section, the framework is implemented on Cases 1-4 to have a comprehensive comparison among cases and recognize what effect EVAs, hydrogen-to-power concept and feeder reconfiguration could have on the volt-var control.

The average voltage profile of the microgrid is illustrated in **Error! Reference source not found.** for all case studies. This figure demonstrates that the proposed volt-var control ensures a safe

 doi:10.20944/preprints202411.0460.v1

operational scheme by maintaining the voltage at the buses within acceptable ranges across all cases. Notably, the voltage profile in Case 3 is flatter than in Cases 1 and 2, which can be attributed to feeder reconfiguration that enhances power sharing among the branches of the microgrid. In Case 4, the hydrogen-to-power-to-hydrogen conversions significantly impact the microgrid's voltage levels, as their functions affect the OLTC tap positions. This adjustment aims to keep the network voltage within acceptable ranges, resulting in higher voltage levels across the network. It can be deduced that feeder reconfiguration in the presence of coordinating other equipment can participate in attaining a flatter voltage profile.

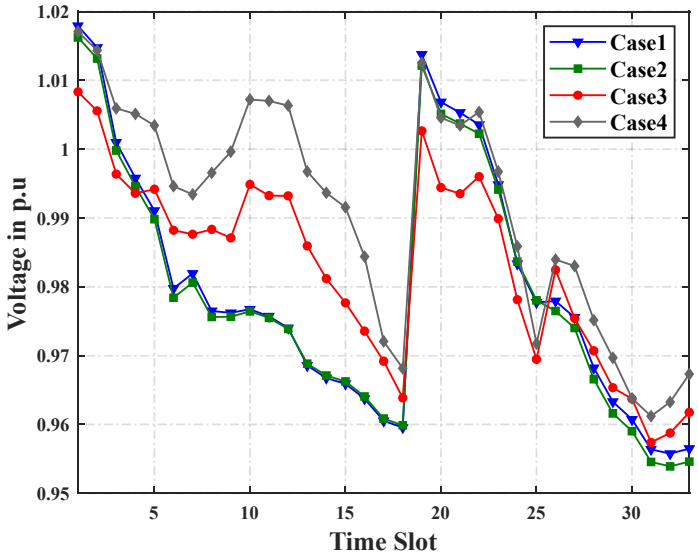

Figure 6. Average voltage of microgrid for different cases.

The operation actions of OLTC are depicted in **Error! Reference source not found.**. The tap position of OLTC in Case 1 is higher than Cases 2 and 3 because of keeping voltage between permissible ranges. However, in Case 2, when EVAs are also coordinated along with other features/equipment, the tap operation of OLTC is decreased in some intervals, e.g., interval [10 15]. The reason is that the EVAs are charged and discharged in the off-peak and peak intervals, respectively, and could compensate for over-/under-voltages; therefore, the OLTC is operated at a lower level. Interestingly, in Case 3, when feeder reconfiguration is also incorporated in the volt-var model, the tap positions decreased more significantly than Cases 1 and 2. Because of changing the microgrid structure, the penetration of RESs and EVA aggregations increased significantly. Consequently, if volt-var is integrated with EVAs and feeder reconfiguration, the OLTC is operated in the lowest positions. The lower tap positions give operators a hand in decreasing the over-voltage issue which occurres during the reverse power flow of PVs. In Case 4, however, the tap position changes more frequently compared to Case 3. This is due to the frequent occurrences of hydrogen-to-power-to-hydrogen conversions, which require the OLTC tap position to be accordingly adjusted to maintain the voltage within acceptable ranges.

Preprints.org (www.preprints.org) | NOT PEER-REVIEWED | Posted: 7 November 2024 doi:10.20944/preprints202411.0460.v1

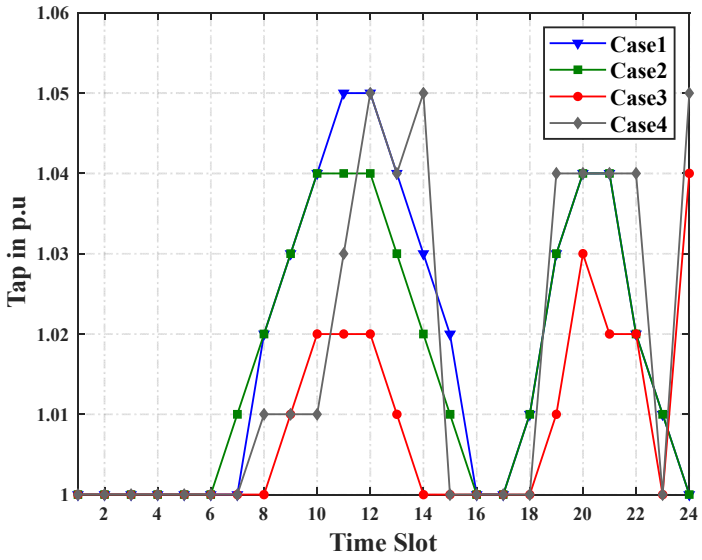

Figure 7. OLTC operation for different cases.

The obtained charge and discharge of EVA throughout the time frame is depicted in **Error! Reference source not found.**. It can be seen that the EVAs are approximately charged from 1 to 7 hours; this corresponds to the off-peak intervals when the electricity price is lower. At the middle interval, from 9 to 15, with a higher market price, the EVAs are discharged to reduce the operational cost. In addition, there are also two hours, comprising 8 and 18, during which EVAs consume energy to transfer the passengers, and thereby, they do not engage with the microgrid. Such a charging/discharging pattern not only satisfies the technical aspects of the microgrid but also could enable the operator to achieve more cost savings.

The reactive power provided by SPIs for Cases 1-4 is illustrated in **Error! Reference source not found.**. From this figure, it is clear that the reactive power management in Case 1 fluctuates significantly from hour 1 to hour 24 to address over-voltage and under-voltage conditions. In Case 2, the reactive power by SPIs experienced a slight change compared to Case 1 because EVAs are charged during hours 1-7, increasing demand and reducing the need for reactive power to address the over-voltage problem. Turning to Case 3, This behavior is attributed to changes because of changing the microgrid's topology, which alters power flows among the branches and enables better sharing of reactive power. Case 4 demonstrates a pattern similar to Case 3, following roughly the same approach to reactive power management.

The committed scheduling of DGs is shown in **Error! Reference source not found.**. It is also noteworthy that the output of the DGs remains relatively stable, with ramp-rate limitations consistently respected throughout the period. The figure clearly indicates that DGs predominantly commit to power generation during hours when market prices are higher, while their generation is constrained during intervals with lower market prices.

 doi:10.20944/preprints202411.0460.v1

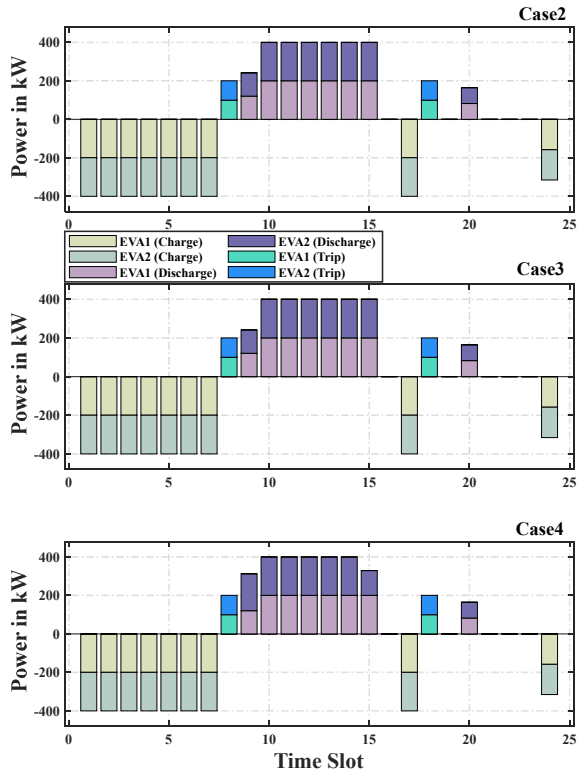

Figure 8. Scheduling of EVAs.

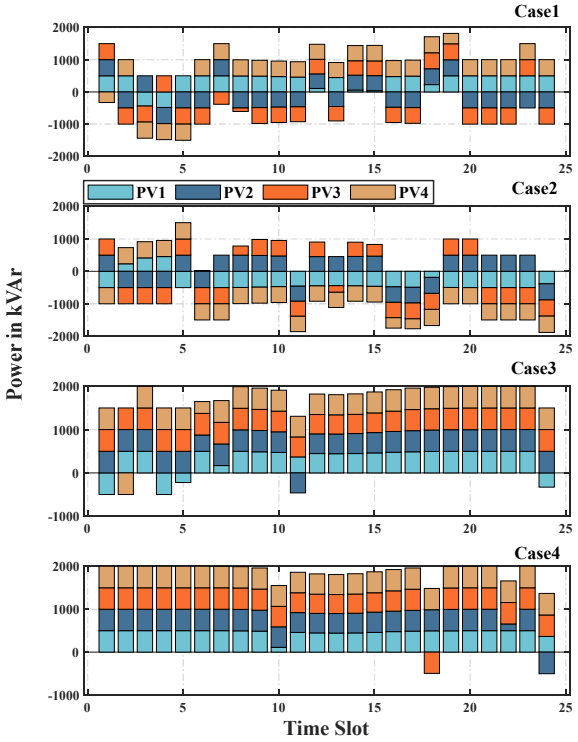

Figure 9. Reactive power scheduling of PV inverters.

 doi:10.20944/preprints202411.0460.v1

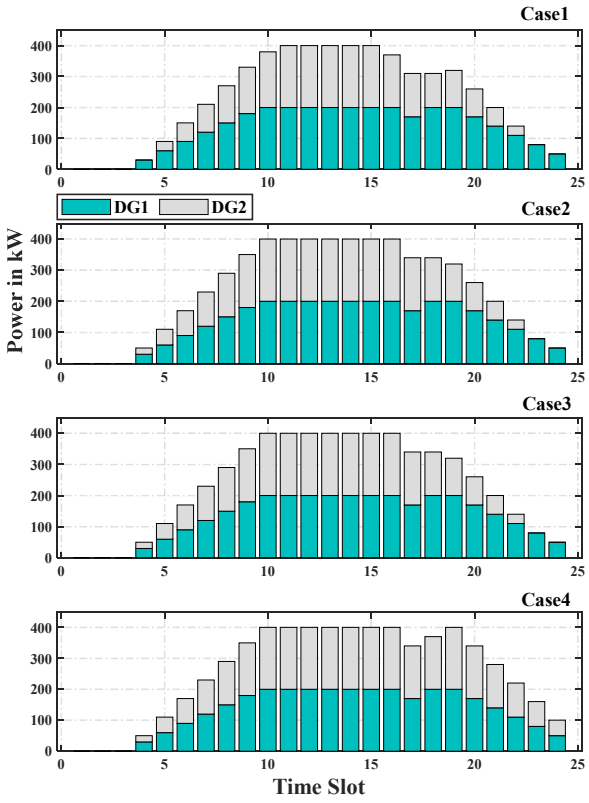

Figure 10. Scheduling of DGs.

Error! Reference source not found. illustrates the operation of two electrolyzers and two fuel cells within the microgrid, emphasizing the P2H and H2P conversions. The electrolyzers generally consume power during hours 1 to 6, specifically taking advantage of lower market prices to charge the hydrogen storage. This stored hydrogen can subsequently be converted back into electricity by the fuel cells, which generate power between hours 10 and 14, when market prices are higher. This sequential operation demonstrates that by shifting power across different intervals, economic benefits are attained.

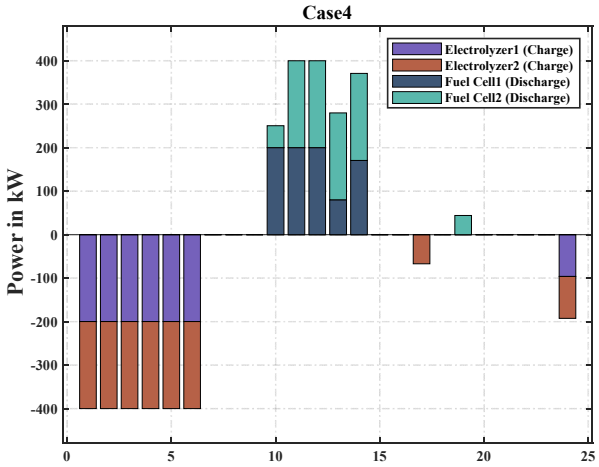

Figure 11. Scheduling of electrolyzer (P2H) and fuel cell (H2P).

 doi:10.20944/preprints202411.0460.v1

Error! Reference source not found. and **Error! Reference source not found.** illustrate the status of switches for the microgrid configuration in Cases 3 and 4, respectively. A noteworthy aspect is that the microgrid configuration changes over time due to the availability and unavailability of various equipment within the timeframe. In other words, adjustments in the penetration of different resources, such as EVAs, electrolyzers, and fuel cells, lead to these changes. Additionally, the configurations in both cases differ because of the incorporation of various resources. This highlights the need to optimize the microgrid topology in the presence of diverse resources to achieve better power sharing and ensure the reliability of technical operations.

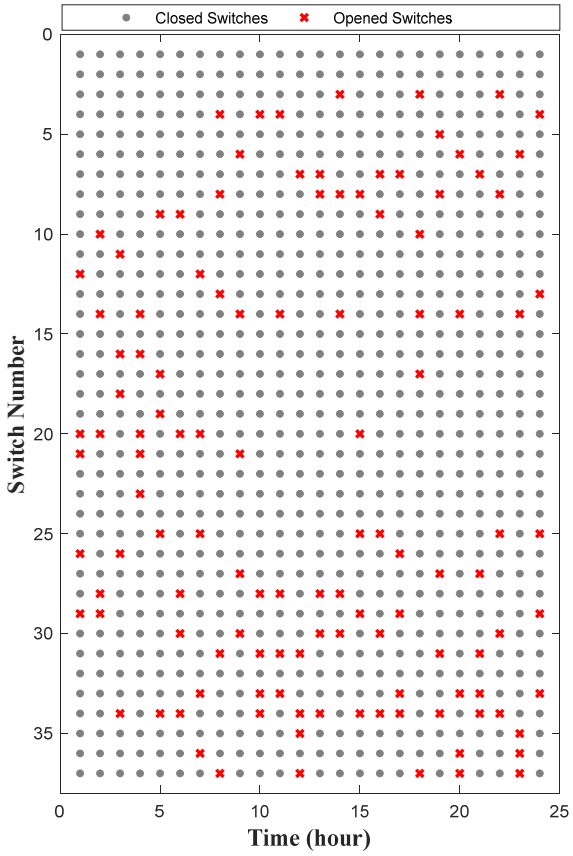

Figure 12. The network configuration in Case 3.

 doi:10.20944/preprints202411.0460.v1

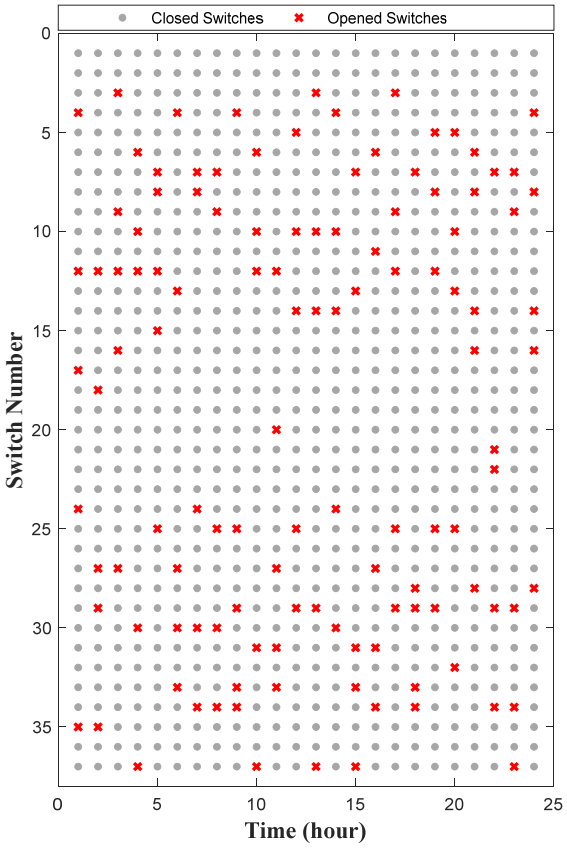

Figure 1. The network configuration in Case 4.

5. Conclusions

This paper introduced a novel volt-var control strategy for reconfigurable microgrids aimed at addressing under-voltage and over-voltage issues. To achieve this, the integration of EVAs, electrolyzers, and fuel cells, along with other volt-var devices, has been carried out in the reconfigurable microgrids.

The results yield several key conclusions. Initially, the operational frequency of OLTCs decreased when considering the simultaneous integration of EVAs and feeder reconfigurations. This indicates that the OLTC operated at a lower level, resulting in a more stable voltage profile across the microgrids. Notably, through optimal coordination of EVAs, both over-voltage and under-voltage occurrences significantly decreased during off-peak and peak intervals. This improvement is attributed to charging EVAs during off-peak hours and discharging them during peak periods. Furthermore, the combination of feeder reconfiguration and EVA coordination enhanced the model flexibility, leading to a flatter voltage profile. The integration of hydrogen conversion technologies contributed to a significant improvement in voltage levels while increasing the operational engagement of the OLTC to maintain voltage within acceptable limits.

Looking ahead, we aim to explore the integration of direct load control demand response mechanisms to further enhance the system's efficiency and responsiveness.

Author Contributions: This will be completed after revision.

Funding: No funds are related to this paper.

Data Availability Statement: The information and data have been cited.

Conflicts of Interest: The authors declare no conflicts of interest.

 doi:10.20944/preprints202411.0460.v1

Nomenclature

Sets, Indexes

$\boldsymbol{\Omega_{par}}$	Set of parent buses
$\boldsymbol{\Omega_{chil}}$	Set of child buses
$\boldsymbol{\Omega_{bus}}$	Set of buses
$\boldsymbol{\Omega_{branch}}$	Set of branches
$\boldsymbol{\Omega_{dg}}$	Set of DGs
$\boldsymbol{\Omega_{PV}}$	Set of SPVIs
$\boldsymbol{\Omega_{eva}}$	Set of EVAs
$\boldsymbol{\Omega_{time}}$	Set of time horizon
$\boldsymbol{\Omega_{up}}$	Set of uncertain parameters
$\boldsymbol{\Omega_{hgn}}$	Set of hydrogen system
$\boldsymbol{\Omega_{cb}}$	Set of capacitor banks
$\boldsymbol{\Omega_{oltc}}$	Set of OLTC
$\boldsymbol{\lvert\Omega_{bus}\rvert}$	The cardinality of the set $\boldsymbol{\Omega_{bus}}$
$\boldsymbol{N(n)}$	The set of buses connected to bus $\boldsymbol{n}$
$\boldsymbol{n, m, k}$	Index of buses
$\boldsymbol{d}$	Index of DGs
$\boldsymbol{e}$	Index of EVA
$\boldsymbol{p}$	Index of SPVIs
$\boldsymbol{c}$	Index of SCBs
$\boldsymbol{t}$	Index of time
$\boldsymbol{o}$	Index of OLTCs
$\boldsymbol{l}$	Indices of sample points
$\boldsymbol{h}$	Index of hydrogen system

Parameters

$\boldsymbol{\lambda_{SS}^{t}}$	Wholesale market price (upstream network)
$\boldsymbol{\lambda_{oltc}^{o}}$	OLTC tap adjustment cost
$\boldsymbol{\lambda_{CB}^{c}}$	Switching cost of capacitor banks
$\boldsymbol{\lambda_{DG}^{d}}$	Operational cost per MWh of DG $\boldsymbol{d}$
$\boldsymbol{E_{eva}^{e,min}}$	Minimum energy for $\boldsymbol{EVA\ e}$
$\boldsymbol{E_{eva}^{e,max}}$	Maximum energy for $\boldsymbol{EVA\ e}$
$\boldsymbol{E_{eva}^{e,initial}}$	Initial energy for $\boldsymbol{EVA\ e}$
$\boldsymbol{E_{eva}^{e,final}}$	Ultimate energy for $\boldsymbol{EVA\ e}$
$\boldsymbol{P_{L}^{n,t}}$	Amount of active power demand at $\boldsymbol{n}$-th bus
$\boldsymbol{P_{DG}^{d,min}}$	Minimum output of DG $\boldsymbol{d}$
$\boldsymbol{P_{DG}^{d,max}}$	Maximum output of DG $\boldsymbol{d}$
$\boldsymbol{P_{ch,eva}^{e,min}}$	Minimum charging of EVA $\boldsymbol{e}$
$\boldsymbol{P_{ch,eva}^{e,max}}$	Maximum charging of EVA $\boldsymbol{e}$
$\boldsymbol{P_{dis,eva}^{e,min}}$	Minimum discharging of EVA $\boldsymbol{e}$

 doi:10.20944/preprints202411.0460.v1

$P_{dis,eva}^{e,max}$	Maximum discharging of EVA e
$P_{FC}^{h,min}$	Minimum generation limit of fuel cell h
$P_{FC}^{h,max}$	Maximum generation limit of fuel cell h
$P_{elsr}^{h,min}$	Minimum consumption limit of electrolyzer h
$P_{elsr}^{h,max}$	Maximum consumption limit of electrolyzer h
$Q_L^{n,t}$	Amount of reactive power demand at n-th bus
Q_{rate}^{c}	The quantity of reactive power by c-th shunt capacitor bank at each step
$R_{DG}^{d,Upper}$	Ramp-up rate of d-th DG
$R_L^{mn,t}$	Branch resistance to connect the bus m to n
$R_{DG}^{d,Down}$	Ramp-up rate of d-th DG
$S_{flow}^{mn,Max}$	Maximum capacity of branch mn to transmit the complex power
S_{PV}^{p}	Inverter rating to connect PV to network
$S_{hgn}^{h,\min}$	Minimum limit of state of hydrogen storage
$S_{hgn}^{h,\max}$	Maximum limit of state of hydrogen storage
$S_{hgn}^{h,t^{final}}$	Final state of hydrogen $(\mathbf{e.g}, t^{final} = \mathbf{24})$
$S_{hgn}^{h,t^{initial}}$	Initial state of hydrogen $(\mathbf{e.g}\ t^{initial} = \mathbf{0})$
$T_{oltc}^{o,min}$	Lower bound of OLTC taps
$T_{oltc}^{o,max}$	Upper bound of OLTC taps
$V_b^{n,min}$	Minimum acceptable voltage at n-th bus
$V_b^{n,max}$	Maximum acceptable voltage at n-th bus
V_{s_0}	Voltage of substation s
W_0	Weight of the mean value μ_x
W_k	Weight of the k-th sample point
$X_L^{mn,t}$	Branch reactance to connect the bus m to n
η_{ch}	Charging efficiency coefficient of EVA
η_{dis}	Discharging efficiency coefficient of EVA
η_{elsr}	Electrolyzer efficiency coefficient
η_{FC}	Fuel cell efficiency coefficient
Δt	Time interval
Ψ_{eih}	Energy density of hydrogen, considered as 39 kWh/kg
$\psi_{CB}^{c,Max}$	Maximum tap setting of the c-th capacitor
$\mathbf{M}_{big}$	A big number

Variables

C_{xx}	Covariance of input uncertain parameters
C_{yy}	Covariance of the output variable Y
$E_{eva}^{e,t}$	Energy of e-th EVA
$H_{elsr}^{h,t}$	The generated hydrogen by electrolyzer h
$H_{FC}^{h,t}$	The consumed hydrogen by fuel cell h
OF	Objective function
$P_{flow}^{mn,t}$	Amount of active power which branch mn carries
P_{SS}^{t}	Amount of power injected into the microgrid via the upstream network

 doi:10.20944/preprints202411.0460.v1

$P_{DG}^{d,t}$	Amount of active power which d-th DG generates
$P_{ch,eva}^{e,t}$	Charging rate of e-th EVA
$P_{dis,eva}^{e,t}$	Discharging rate of e-th EVA
$P_{net}^{n,t}$	Summation of active loads and generations at n-th bus
$P_{PV}^{p,t}$	Amount of active power generated by p-th PV resource
$P_{elsr}^{h,t}$	Consumed power by h-th electrolyzer
$P_{FC}^{h,t}$	Generated power by h-th fuel cell
$Q_{flow}^{mn,t}$	Amount of reactive power which branch mn carries
$Q_{DG}^{d,t}$	Amount of reactive power which d-th DG generates
$Q_{PV}^{p,t}$	Amount of reactive power generated by p-th PV resource
$Q_{net}^{n,t}$	Summation of reactive loads and generations at n-th bus
$Q_{CB}^{c,t}$	Amount of reactive power which c-th switchable capacitor bank provides
$S_{hgn}^{h,t}$	State of charge of hydrogen storage h
$\varphi^{m,n}, \varphi^{n,m}$	Binary variables that indicate parent-child relationship indices.
$\alpha^{mn,t}$	Status of branch mn at time t (Open switches are represented by 0, while closed switches are represented by 1)
S_p^l	l-th sample observation of uncertain parameters
Y^l	Value of the fitness function at the l-th sample observation
$Tap_{oltc}^{o,t}$	Step of o-th OLTC
$V_b^{n,t}$	Voltage of bus n
$\psi_{CB}^{c,t}$	Integer variable taking the steps of c-th switchable capacitor bank
μ_x	Average value of input uncertain parameters
μ_y	Average value of the output variable Y

Abbreviation

P2H	Power to hydrogen
H2P	Hydrogen to power
DGs	Diesel generators
EVA	Electric vehicle aggregation
OLTC	On-line tap changer transformer
PV	Photovoltaic array
RESs	Renewable energy sources
SCBs	Switchable capacitor banks
SPIs	Smart PV inverters
Volt-VAr	Voltage-volt Ampere Reactive
VVC	Volt-VAr control
UT	Unscented transformation
PDF	Probability distribution function

 doi:10.20944/preprints202411.0460.v1

References

1. Hemmatpour, M.H.; Mohammadian, M.; Gharaveisi, A.A. Optimum Islanded Microgrid Reconfiguration Based on Maximization of System Loadability and Minimization of Power Losses. *Int. J. Electr. Power Energy Syst.* **2016**, *78*, 343–355, doi:10.1016/j.ijepes.2015.11.040.
2. Boland, J.; Filar, J.A.; Mohammadian, G.; Nazari, A. Australian Electricity Market and Price Volatility. *Ann. Oper. Res.* **2016**, *241*, 357–372, doi:10.1007/s10479-011-1033-x.
3. Aryanezhad, M. Management and Coordination of LTC, SVR, Shunt Capacitor and Energy Storage with High PV Penetration in Power Distribution System for Voltage Regulation and Power Loss Minimization. *Int. J. Electr. Power Energy Syst.* **2018**, *100*, 178–192, doi:10.1016/j.ijepes.2018.02.015.
4. Liu, J.; Li, Y.; Rehtanz, C.; Cao, Y.; Qiao, X.; Lin, G.; Song, Y.; Sun, C. An OLTC-Inverter Coordinated Voltage Regulation Method for Distribution Network with High Penetration of PV Generations. *Int. J. Electr. Power Energy Syst.* **2019**, *113*, 991–1001, doi:10.1016/j.ijepes.2019.06.030.
5. Abbas, A.S.; El-Sehiemy, R.A.; Abou El-Ela, A.; Ali, E.S.; Mahmoud, K.; Lehtonen, M.; Darwish, M.M.F. Optimal Harmonic Mitigation in Distribution Systems with Inverter Based Distributed Generation. *Appl. Sci.* **2021**, *11*, 1–16, doi:10.3390/app11020774.
6. Zafar, R.; Ravishankar, J.; Fletcher, J.E.; Pota, H.R. Multi-Timescale Voltage Stability-Constrained Volt/VAR Optimization with Battery Storage System in Distribution Grids. *IEEE Trans. Sustain. Energy* **2020**, *11*, 868–878, doi:10.1109/TSTE.2019.2910726.
7. Prabpal, P.; Kongjeen, Y.; Bhumkittipich, K. Optimal Battery Energy Storage System Based on VAR Control Strategies Using Particle Swarm Optimization for Power Distribution System. *Symmetry (Basel).* **2021**, *13*, 1692, doi:10.3390/sym13091692.
8. Pamshetti, V.B.; Singh, S.; Thakur, A.K.; Singh, S.P. Multistage Coordination Volt/VAR Control with CVR in Active Distribution Network in Presence of Inverter-Based DG Units and Soft Open Points. *IEEE Trans. Ind. Appl.* **2021**, *57*, 2035–2047, doi:10.1109/TIA.2021.3063667.
9. Gholami, K.; Azizivahed, A.; Arefi, A.; Li, L. Risk-Averse Volt-VAr Management Scheme to Coordinate Distributed Energy Resources with Demand Response Program. *Int. J. Electr. Power Energy Syst.* **2023**, *146*, 108761, doi:10.1016/j.ijepes.2022.108761.
10. Sabillon-Antunez, C.; Melgar-Dominguez, O.D.; Franco, J.F.; Lavorato, M.; Rider, M.J. Volt-VAr Control and Energy Storage Device Operation to Improve the Electric Vehicle Charging Coordination in Unbalanced Distribution Networks. *IEEE Trans. Sustain. Energy* **2017**, *8*, 1560–1570, doi:10.1109/TSTE.2017.2695195.
11. Tushar, M.H.K.; Assi, C. Volt-VAR Optimization by Using Electric Vehicle, Renewable Energy and Residential Load-Shifting. *2016 IEEE Int. Conf. Smart Grid Commun. SmartGridComm 2016* **2016**, 460–465, doi:10.1109/SmartGridComm.2016.7778804.
12. Gholami, K.; Karimi, S.; Rastgou, A.; Nazari, A.; Moghaddam, V. Voltage Stability Improvement of Distribution Networks Using Reactive Power Capability of Electric Vehicle Charging Stations. *Comput. Electr. Eng.* **2024**, *116*, doi:10.1016/j.compeleceng.2024.109160.
13. Nandhakumar, S.K.; Muthukumar, R. Combined Reconfiguration and Capacitor Placement for Distribution System Volt/Var Control through Opposition Based Differential Evolution Algorithm. *Automatika* **2015**, *56*, 140–148, doi:10.7305/automatika.2015.07.611.
14. Pamshetti, V.B.; Singh, S.; Singh, S.P. Combined Impact of Network Reconfiguration and Volt-VAR Control Devices on Energy Savings in the Presence of Distributed Generation. *IEEE Syst. J.* **2020**, *14*, 995–1006, doi:10.1109/JSYST.2019.2928139.
15. Microgrid, D. Volt – Var Optimization and Reconfiguration : Reducing Power Demand and Losses in A. **2021**, *57*, 2769–2781.
16. Guo, X.; Zhu, H.; Zhang, S. Overview of Electrolyser and Hydrogen Production Power Supply from Industrial Perspective. *Int. J. Hydrogen Energy* **2024**, *49*, 1048–1059, doi:10.1016/j.ijhydene.2023.10.325.
17. Massaro, M.C.; Biga, R.; Kolisnichenko, A.; Marocco, P.; Monteverde, A.H.A.; Santarelli, M. Potential and Technical Challenges of On-Board Hydrogen Storage Technologies Coupled with Fuel Cell Systems for Aircraft Electrification. *J. Power Sources* **2023**, *555*, doi:10.1016/j.jpowsour.2022.232397.
18. Ghaithan, A.M.; Kondkari, M.; Mohammed, A.; Attia, A.M. Optimal Design of Concentrated Solar Power-Based Hydrogen Refueling Station: Mixed Integer Linear Programming Approach. *Int. J. Hydrogen Energy* **2024**, *86*, 703–718, doi:10.1016/j.ijhydene.2024.08.451.

19. Shahbazbegian, V.; Shafie-khah, M.; Laaksonen, H.; Strbac, G.; Ameli, H. Resilience-Oriented Operation of Microgrids in the Presence of Power-to-Hydrogen Systems. *Appl. Energy* **2023**, *348*, doi:10.1016/j.apenergy.2023.121429.
20. Yu, N.; Duan, W.; Fan, X. Hydrogen-Fueled Microgrid Energy Management: Novel EMS Approach for Efficiency and Reliability. *Int. J. Hydrogen Energy* **2024**, doi:10.1016/j.ijhydene.2024.05.434.
21. Zhang, W.; Gandhi, O.; Quan, H.; Rodríguez-Gallegos, C.D.; Srinivasan, D. A Multi-Agent Based Integrated Volt-Var Optimization Engine for Fast Vehicle-to-Grid Reactive Power Dispatch and Electric Vehicle Coordination. *Appl. Energy* **2018**, *229*, 96–110, doi:10.1016/j.apenergy.2018.07.092.
22. Malekpour, A.R.; Niknam, T. A Probabilistic Multi-Objective Daily Volt/Var Control at Distribution Networks Including Renewable Energy Sources. *Energy* **2011**, *36*, 3477–3488, doi:10.1016/j.energy.2011.03.052.
23. Baghaee, H.R.; Mirsalim, M.; Gharehpetian, G.B.; Talebi, H.A. Application of RBF Neural Networks and Unscented Transformation in Probabilistic Power-Flow of Microgrids Including Correlated Wind/PV Units and Plug-in Hybrid Electric Vehicles. *Simul. Model. Pract. Theory* **2017**, *72*, 51–68, doi:10.1016/j.simpat.2016.12.006.
24. Dabbaghjamanesh, M.; Kavousi-Fard, A.; Mehraeen, S. Effective Scheduling of Reconfigurable Microgrids With Dynamic Thermal Line Rating. *IEEE Trans. Ind. Electron.* **2019**, *66*, 1552–1564, doi:10.1109/TIE.2018.2827978.
25. Jashfar, S.; Esmaeili, S. Volt/Var/THD Control in Distribution Networks Considering Reactive Power Capability of Solar Energy Conversion. *Int. J. Electr. Power Energy Syst.* **2014**, *60*, 221–233, doi:10.1016/j.ijepes.2014.02.038.
26. Ameli, A.; Ahmadifar, A.; Shariatkhah, M.H.; Vakilian, M.; Haghifam, M.R. A Dynamic Method for Feeder Reconfiguration and Capacitor Switching in Smart Distribution Systems. *Int. J. Electr. Power Energy Syst.* **2017**, *85*, 200–211, doi:10.1016/j.ijepes.2016.09.008.
27. Emarati, M.; Barani, M.; Farahmand, H.; Aghaei, J.; del Granado, P.C. A Two-Level over-Voltage Control Strategy in Distribution Networks with High PV Penetration. *Int. J. Electr. Power Energy Syst.* **2021**, *130*, 106763, doi:10.1016/j.ijepes.2021.106763.
28. Arunachalam, M.; Yoo, Y.; Al-Ghamdi, A.S.; Park, H.; Han, D.S. Integrating Green Hydrogen Production with Renewable Energy-Powered Desalination: An Analysis of CAPEX Implications and Operational Strategies. *Int. J. Hydrogen Energy* **2024**, *84*, 344–355, doi:10.1016/j.ijhydene.2024.08.250.
29. Li, M.; Bai, Y.; Zhang, C.; Song, Y.; Jiang, S.; Grouset, D.; Zhang, M. Review on the Research of Hydrogen Storage System Fast Refueling in Fuel Cell Vehicle. *Int. J. Hydrogen Energy* **2019**, *44*, 10677–10693, doi:10.1016/j.ijhydene.2019.02.208.
30. Mehrjerdi, H. Off-Grid Solar Powered Charging Station for Electric and Hydrogen Vehicles Including Fuel Cell and Hydrogen Storage. *Int. J. Hydrogen Energy* **2019**, *44*, 11574–11583, doi:10.1016/j.ijhydene.2019.03.158.
31. Pamshetti, V.B.; Singh, S.; Thakur, A.K.; Singh, S.P. Multistage Coordination Volt/VAR Control with CVR in Active Distribution Network in Presence of Inverter-Based DG Units and Soft Open Points. *IEEE Trans. Ind. Appl.* **2021**, *57*, 2035–2047, doi:10.1109/TIA.2021.3063667.
32. Yuan, W.; Wang, J.; Qiu, F.; Chen, C.; Kang, C.; Zeng, B. Robust Optimization-Based Resilient Distribution Network Planning Against Natural Disasters. *IEEE Trans. Smart Grid* **2016**, *7*, 2817–2826, doi:10.1109/TSG.2015.2513048.
33. Javadi, M.S.; Esmaeel Nezhad, A.; Jordehi, A.R.; Gough, M.; Santos, S.F.; Catalão, J.P.S. Transactive Energy Framework in Multi-Carrier Energy Hubs: A Fully Decentralized Model. *Energy* **2022**, *238*, 121717, doi:10.1016/j.energy.2021.121717.
34. Dorostkar-Ghamsari, M.R.; Fotuhi-Firuzabad, M.; Lehtonen, M.; Safdarian, A. Value of Distribution Network Reconfiguration in Presence of Renewable Energy Resources. *IEEE Trans. Power Syst.* **2016**, *31*, 1879–1888, doi:10.1109/TPWRS.2015.2457954.
35. Guo, Z.; Zhou, Z.; Zhou, Y. Impacts of Integrating Topology Reconfiguration and Vehicle-to-Grid Technologies on Distribution System Operation. *IEEE Trans. Sustain. Energy* **2020**, *11*, 1023–1032, doi:10.1109/TSTE.2019.2916499.
36. Mohseni, M.; Joorabian, M.; Lashkar Ara, A. Distribution System Reconfiguration in Presence of Internet of Things. *IET Gener. Transm. Distrib.* **2021**, *15*, 1290–1303, doi:10.1049/gtd2.12102.

 doi:10.20944/preprints202411.0460.v1

37. Moghari, P.; Chabanloo, R.M.; Torkaman, H. Distribution System Reconfiguration Based on MILP Considering Voltage Stability. *Electr. Power Syst. Res.* **2023**, *222*, doi:10.1016/j.epsr.2023.109523.
38. Jabr, R.A.; Singh, R.; Pal, B.C. Minimum Loss Network Reconfiguration Using Mixed-Integer Convex Programming. *IEEE Trans. Power Syst.* **2012**, *27*, 1106–1115, doi:10.1109/TPWRS.2011.2180406.
39. Kavousi-Fard, A.; Niknam, T.; Fotuhi-Firuzabad, M. Stochastic Reconfiguration and Optimal Coordination of V2G Plug-in Electric Vehicles Considering Correlated Wind Power Generation. *IEEE Trans. Sustain. Energy* **2015**, *6*, 822–830, doi:10.1109/TSTE.2015.2409814.
40. Aien, M.; Fotuhi-Firuzabad, M.; Aminifar, F. Probabilistic Load Flow in Correlated Uncertain Environment Using Unscented Transformation. *IEEE Trans. Power Syst.* **2012**, *27*, 2233–2241, doi:10.1109/TPWRS.2012.2191804.
41. Gholami, K.; Jazebi, S. Energy Demand and Quality Management of Standalone Diesel/PV/Battery Microgrid Using Reconfiguration. *Int. Trans. Electr. Energy Syst.* **2020**, *30*, 1–21, doi:10.1002/2050-7038.12550.